2015

Temporal dynamics of groundwater-dissolved inorganic carbon beneath a drought-affected braided stream: Platte River case study

Audrey R. Boerner
University of Nebraska-Lincoln, aboerner@huskers.unl.edu

John B. Gates
The Climate Corporation

AGU PUBLICATIONS

JGR

Journal of Geophysical Research: Biogeosciences

RESEARCH ARTICLE
10.1002/2015JG002950

Key Points:
- Water chemistry documented beneath vegetated and nonvegetated fluvial islands
- Increasing soil pCO_2 during river drying impacted groundwater carbonate system
- Evaporation effect on pore water was small compared to soil/CO_2/water effects

Supporting Information:
- Figures S1 and S2
- Table S1

Correspondence to:
A. R. Boerner,
aboerner2@gmail.com

Citation:
Boerner, A. R., and J. B. Gates (2015), Temporal dynamics of groundwater-dissolved inorganic carbon beneath a drought-affected braided stream: Platte River case study, *J. Geophys. Res. Biogeosci.*, *120*, 924–937, doi:10.1002/2015JG002950.

Received 9 FEB 2015
Accepted 14 APR 2015
Accepted article online 21 APR 2015
Published online 19 MAY 2015

Temporal dynamics of groundwater-dissolved inorganic carbon beneath a drought-affected braided stream: Platte River case study

Audrey R. Boerner[1] and John B. Gates[2]

[1]Department of Earth and Atmospheric Sciences, University of Nebraska-Lincoln, Lincoln, Nebraska, USA, [2]The Climate Corporation, San Francisco, California, USA

Abstract Impacts of environmental changes on groundwater carbon cycling are poorly understood despite their potentially high relevance to terrestrial carbon budgets. This study focuses on streambed groundwater chemistry during a period of drought-induced river drying and consequent disconnection between surface water and groundwater. Shallow groundwater underlying vegetated and bare portions of a braided streambed in the Platte River (Nebraska, USA) was monitored during drought conditions in summer 2012. Water temperature and dissolved inorganic carbon (dominated by HCO_3^-) in streambed groundwater were correlated over a 3 month period coinciding with a decline in river discharge from 35 to 0 $m^3 s^{-1}$. Physical, chemical, and isotopic parameters were monitored to investigate mechanisms affecting the HCO_3^- trend. Equilibrium thermodynamic modeling suggests that an increase of pCO_2 near the water table, coupled with carbonate mineral weathering, can explain the trend. Stronger temporal trends in Ca^{2+} and Mg^{2+} compared to Cl^- are consistent with carbonate mineral reequilibria rather than evaporative concentration as the primary mechanism of the increased HCO_3^-. Stable isotope trends are not apparent, providing further evidence of thermodynamic controls rather than evaporation from the water table. A combination of increased temperature and O_2 in the dewatered portion of the streambed is the most likely driver of increased pCO_2 near the water table. Results of this study highlight potential linkages between surface environmental changes and groundwater chemistry and underscore the need for high-resolution chemical monitoring of alluvial groundwater in order to identify environmental change impacts.

1. Introduction

Dissolved inorganic carbon (DIC) in groundwater is a poorly constrained, though potentially significant, component of the terrestrial carbon budget [*Kessler and Harvey*, 2001; *Cole et al.*, 2007; *Macpherson*, 2009]. Constraints on groundwater DIC are important for estimation of the carbon budgets of rivers and oceans [*Raymond and Cole*, 2003; *Worrall and Lancaster*, 2005; *Jahangir et al.*, 2012; *Lauerwald et al.*, 2013]. Groundwater can also be a source of CO_2 to the atmosphere through degassing at surface seeps and springs and as a result of groundwater pumping [*Richey et al.*, 2009]. In addition to carbon cycles, groundwater DIC is important to consider because of its influence on other water quality parameters including metals and pH [*Appelo et al.*, 2002; *Xie et al.*, 2012].

Although the degree to which environmental changes affect DIC in aquifers on a global basis is not known, several case studies have demonstrated strong links between temperature and groundwater DIC fluctuations [*Drake and Wigley*, 1975; *Andrews and Schlesinger*, 2001; *Macpherson et al.*, 2008; *Liu et al.*, 2010; *Yan et al.*, 2011]. Improved understanding of links between temperature and groundwater DIC is especially critical given the need to predict impacts of climate change, including the anticipated increase in intensity and frequency of North American heat waves [*Meehl and Tebaldi*, 2004] on the carbon cycle. For example, there is ongoing debate as to whether drought and increased temperatures will increase or decrease global CO_2 sinks [*Borken et al.*, 1999; *Cornic and Fresneau*, 2002; *Ciais et al.*, 2005; *Zeng and Qian*, 2005; *Liu et al.*, 2010; *Zhao and Running*, 2010; *Medlyn*, 2011]. Longstanding attention has been paid to the indirect links between temperature and groundwater DIC as a result of the temperature dependence of carbonate mineral solubility and CO_2 solubility [*Drake and Wigley*, 1975; *Liu and Zhao*, 1999; *Yan et al.*, 2011; *Tsypin and Macpherson*, 2012]. More recently, studies have identified potential links between temperature, soil gas CO_2, and groundwater DIC. For example, *Macpherson et al.* [2008] found a 20% increase in

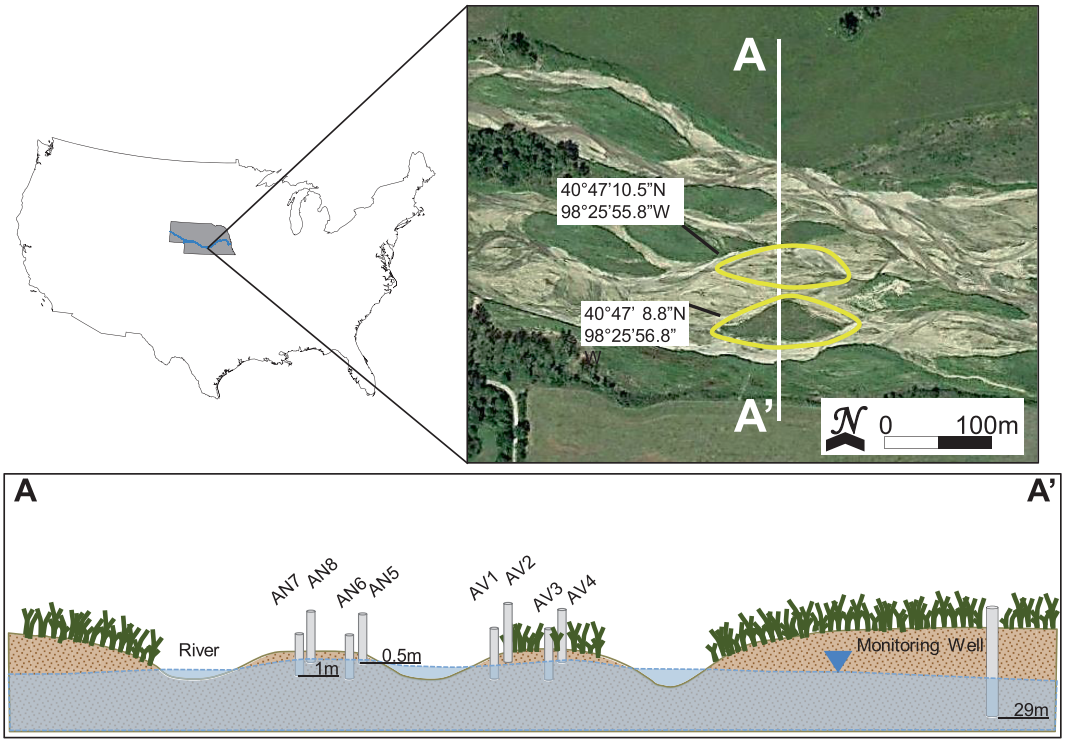

Figure 1. Study location on the Platte River, Nebraska, USA. Two piezometer nests were installed on vegetated and nonvegetated islands. On the cross section, note piezometers AV1-4 are installed on a vegetated island, AN5-8 in the nonvegetated island. Depths of piezometers and monitoring well are given. Cross section is not to scale. Image source: U.S. Department of Agriculture Farm Service Agency.

groundwater CO_2 over a 15 year study; the authors suggest that the forcing mechanism may be related to increased soil respiration as a result of increased air temperature.

This study addresses hydrochemical trends in shallow groundwater during a period of drought-induced groundwater table decline and a concurrent seasonal temperature increase, with a focus on the carbonate system. The objective of this study was to quantify chemical changes in shallow groundwater (upper 1 m of the saturated zone) in the lower Platte River during an extreme drought and extended high-temperature period in summer 2012. The June 2012 through August 2012 precipitation record in Nebraska (northern High Plains region, USA) was the driest over the 118 year record [*National Climatic Data Center (NCDC)*, 2014]. The rationale for focusing on streambed groundwater during drought is based on extensive evidence that hyporheic zone processes are both temporally dynamic and highly influential on many aspects of water quality [*Brunke and Gonser*, 1997; *Boulton et al.*, 1998]. Assessment of changes to hyporheic zone processes during periods of drought and elevated temperature may offer a potential analog for trends associated with future climate extremes.

2. Methods

2.1. Study Area

This study took place within a stable branch of the Platte River in the northern High Plains region, USA, approximately 240 km west of Omaha, Nebraska (Figure 1). The Platte River watershed is approximately 222,740 km^2 and includes portions of Colorado, Wyoming, and Nebraska [*Eschner et al.*, 1983]. The Platte River is a well-known example of a braided river system, which generally represents unstable channel conditions in which the channel bottom is under active construction [*Piégay et al.*, 2006] and subject to significant morphologic change during high-flow regimes [*Lane*, 1995; *Eaton et al.*, 2010]. A braided river pattern develops under high-sediment load and high-streambed slope conditions in which the river's sediment load exceeds its carrying capacity [*Leopold and Wolman*, 1957; *Piégay et al.*, 2006]. This model of

active construction and the unstable nature of the channel bed can lead to coexisting stable, vegetated islands and transient, nonvegetated gravel bars within a single channel [*Piégay et al.*, 2006]. Stable, vegetated islands are a ubiquitous feature of Platte River geomorphology. The islands and bars in the Platte River vary greatly in size, ranging from 7 m to 405 m long and 3 m to 91 m wide [*Horn et al.*, 2012]. The Platte River is characteristically shallow (<1 m), with banks a few meters high [*Williams*, 1978]. Dense vegetation is present along the banks of the river, ranging from scrub brush to willow and cottonwood trees. Trees and dense brushes are also present on many of the islands within the channel.

Anthropogenic influences in the Platte basin include dams, hydroelectric diversion canals, and a high density of irrigation wells [*Chen*, 2007], which have reduced mean annual flows in the river. Reaches in the most heavily irrigated areas regularly become dry during summer [*Hurr*, 1983; *Chen*, 2007]. The alluvial aquifer adjacent to the Platte River channel comprises Pliocene and Pleistocene alluvial sediments deposited during Platte River migration. At the study's monitoring location (Figure 1), the alluvial deposits include unconsolidated sediments of widely varying textures and are approximately 45 m thick and laterally continuous [*Chen*, 2007, 2011]. Streambed sediments are mostly poorly sorted sands and gravels, with finer sediments present in low-energy pools and on stable islands. Streambed sediments have been estimated to have vertical hydraulic conductivities of 25 to 45 m d^{-1} [*Cheng et al.*, 2011; *Chen*, 2011; *Chen et al.*, 2013] and horizontal hydraulic conductivities of 100 to 120 m d^{-1} at the surface [*Chen and Shu*, 2006]. Groundwater flow is approximately parallel to the river channel [*Chen and Shu*, 2006], and hydraulic gradients between the river and groundwater vary seasonally and spatially [*Peckenpaugh and Dugan*, 1983; *Kilpatrick*, 1996].

Two adjacent islands (one vegetated, ~70 m long, ~40 m wide; one nonvegetated, ~50 m long, ~20 m wide) were monitored over the period of 23 May 2012 to 22 August 2012 (40°47′8.8″N, 98°25′56.8″W; 40°47′10.5″N, 98°25′55.8″W; Figure 1). The Platte River along this reach is separated into three channels (i.e., anabranches, referred to as North, Middle, and South Channels). The islands selected for this study were within the South Channel. The distance between the North Channel and South Channel is 3200 m (the total width of the three individual channels at this location is ~300 m). The study area is heavily agricultural, with a mix of irrigated cropland and pastureland. The nearest city, Grand Island, Nebraska, is approximately 11 km downstream of the study site.

The 30 year mean annual precipitation for the area is 650 mm. However, in the 12 month period beginning 1 September 2011 to the conclusion of this study in August 2012, 390 mm of precipitation was recorded, which is 40% less than the mean annual precipitation. The Palmer Drought Severity Index indicated mild drought conditions in May 2012 (−1.90), which became extreme in July (−4.60) and August (−5.48) [*NCDC*, 2013]. Daily stream discharge over the study period ranked in the 23rd percentile of daily flows for the 78 year discharge record (U.S. Geological Survey (USGS) stream gauge 06770500; Figure 2a).

2.2. Experimental Infrastructure

Nine piezometers were installed in a north-south transect perpendicular to river flow to monitor groundwater levels and provide sampling access (Figure 1; 6 cm threaded PVC, 0.2 m screen interval). One piezometer was installed in the river bed, and four piezometers were installed in each island. Each island contained paired piezometers screened at 0.5 m and 1 m below surface in order to determine vertical hydraulic gradients. Both islands contained one nest in the center of the island and one nest at the edge. This experimental configuration allowed for redundant piezometer pairs on both islands and the ability to collect representative samples from both the vegetated and nonvegetated island. Despite inherent heterogeneity in this system, the results indicate that this number of sampling points was sufficient for the size of the islands. Additional samples were collected from the river channel and a monitoring well 1 km south of the study site with a screen depth approximately 29 m below the surface.

All piezometers except AV2 were initially screened below the water table, although some piezometers became temporarily dry over the sampling period due to water table decline. An unvented pressure transducer (Solinst Levelogger Edge 3001 F5/M15) was suspended in each piezometer by Kevlar cord to record water level and temperature fluctuations in 2 min increments. One barometric pressure transducer (Solinst Barologger Edge 3001) was also deployed in piezometer AV4 to compensate water level data for barometric pressure fluctuations. Vertical hydraulic gradients (VHGs) were calculated for three piezometer

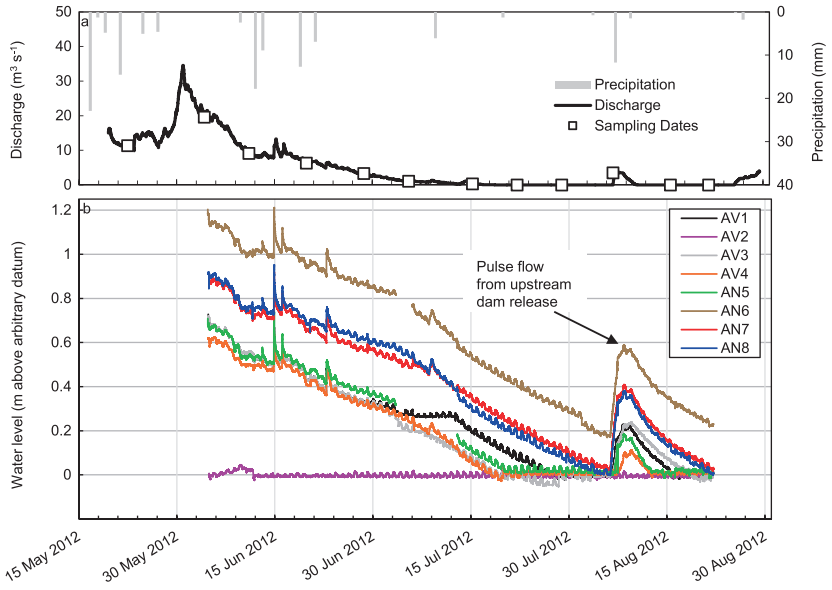

Figure 2. (a) Streamflow recorded at the USGS gaging station 06770500. Precipitation data are from the National Climatic Data Center, recorded in Grand Island, Nebraska. Following a period of high flow in early June, river stage declined steadily until the channel became dry in mid-July. The brief flow in early August represents an upstream dam release. (b) Water level measured by pressure transducers in the island piezometers. All piezometers indicate diurnal fluctuations in the water table. The early August peak recorded in all piezometers was due to an upstream dam release. Piezometer AV2 was installed dry and remained dry throughout the study. The water level fluctuation in this piezometer is likely due to diurnal fluctuations in the capillary fringe.

pairs; two pairs were located on the nonvegetated island and one pair was located on the vegetated island. VHGs were calculated as $\Delta h/\Delta L$, in which Δh represents the difference in total hydraulic head, and ΔL represents the difference in screen-top elevation above an arbitrary datum.

2.3. Chemical Methods

Prior to sampling, each piezometer was purged with a portable peristaltic pump until stabilization of dissolved oxygen, temperature, and electrical conductivity in a flow cell (YSI ProPlus meter with Quatro sonde, Yellow Springs, OH, USA). Oxidation-reduction potential (ORP) was also measured by the multiparameter meter at this time (calibrations for all parameters were done within 8 h of sampling in all cases; one-point Zobell's solution calibration for ORP; three-point buffer solution calibration for pH, two-point standard calibration for conductivity; and one-point water-saturated air calibration for dissolved oxygen). The manufacturer's reported accuracy for these parameters is as follows: temperature = ±0.2°C, pH = ±0.2 units, ORP = ±20 mV, O_2 = ±2% of reading or 0.2 mg/L, whichever is greater. Total alkalinity was estimated at the sampling location by H_2SO_4 titration to approximately pH 4.5. Samples collected for major ion and stable isotope analyses were filtered through a 0.45 μm nylon filter into 8 mL high density polyethylene bottles and immediately chilled. Cation samples were also acidified with HNO_3 to pH $<$2. Major anions (Cl^-, SO_4^{2-}, and NO_3^-) and cations (Ca^{2+}, Mg^{2+}, Na^+, and K^+) were analyzed via ion chromatography (Dionex ICS-2100 with five- and four-standard calibrations, respectively; analytical accuracy $<$10% of concentration in all cases; method detection limit = 0.1 mg L^{-1}). Samples for stable isotopes of water ($\delta^{18}O$ and δ^2H) were filtered and were analyzed using a Picarro Cavity Ringdown Spectrometer (analytical accuracy = ±0.2 $\delta^{18}O$‰, ±2 δ^2H‰ Vienna SMOW).

2.4. Thermodynamic Modeling Procedures

The thermodynamic equilibrium model PHREEQC [*Parkhurst and Appelo*, 1999] was used to determine carbon speciation in solution and carbonate mineral saturation indices using field-measured temperature, pH, and total alkalinity estimated from field titration as constraints. Total alkalinity was assumed equal to carbonate alkalinity, as concentrations of other alkalinity-producing ions or organic acids are likely to be very low [*Williams et al.*, 2009]. Since HCO_3^- is the dominant carbonate ion species in water with a pH between 6.4 and 10.3, and all

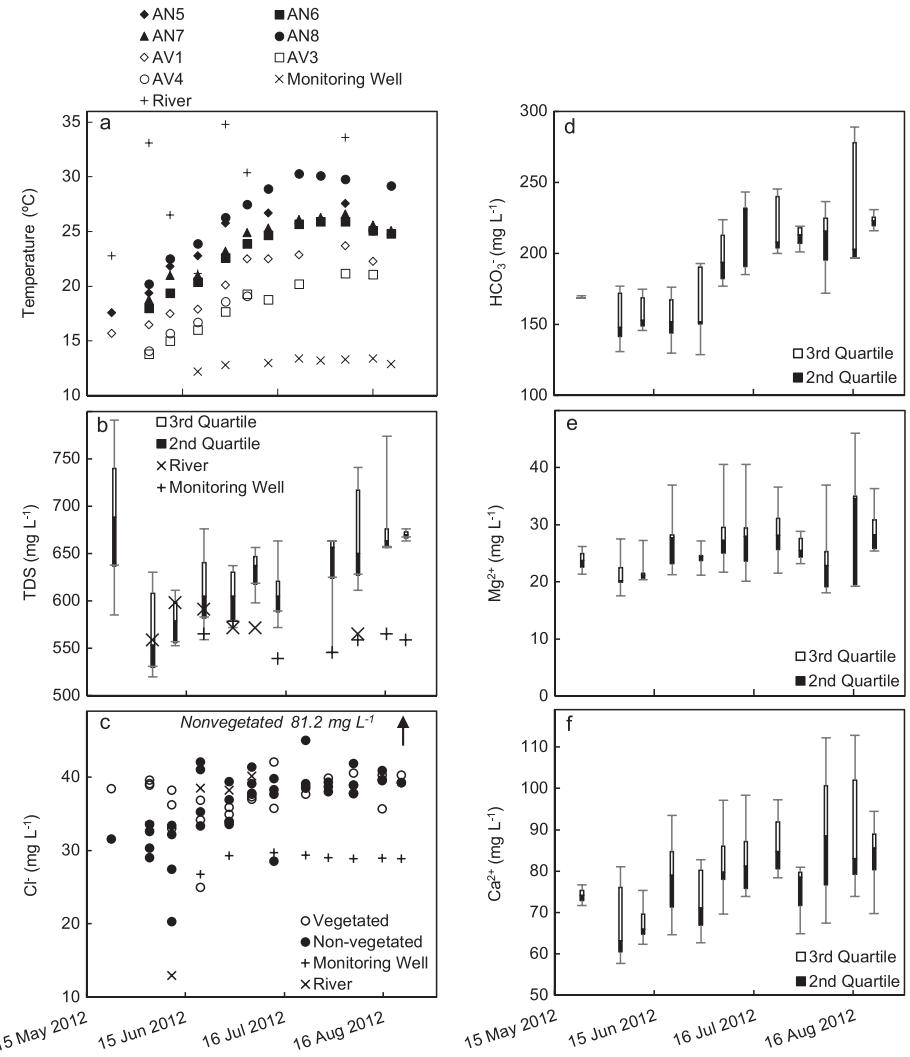

Figure 3. Time series of water temperature and major ions. On box-and-whisker plots, the upper and lower bars represent the minimum and maximum measurement for that date. The shaded box represents the 25th to 50th percentile, the hollow box represents the 50th to 75th percentiles. (a) Temperature increased steadily in the piezometers until middle to late July, after which it stabilized. Vegetated island shallow groundwater temperatures were relatively cooler than the nonvegetated for the entire study period. The deeper piezometers of each nest were also cooler than the shallow piezometer in the same nest. Groundwater temperatures were relatively stable throughout the study period. River water temperature fluctuated and is likely influenced by the time of day temperature measurements were collected. (b) Total dissolved solids increased over the study period in the vegetated and nonvegetated islands. River and monitoring well data do not show a temporal trend. (c) Chloride concentration in the islands and monitoring well remained stable after an initial increase in June. (d–f) Major carbonate system ions increased over the study period. The greatest increase was measured in HCO_3^- concentration followed by Ca^{2+} and Mg^{2+}.

island samples contained a pH between 7.2 and 8.1, CO_3^{2-} is not considered here (see pH time series in the supporting information). Therefore, HCO_3^- is assumed to be the dominant contributor to alkalinity. Modeling details are described in the discussion section. The approach uses the extended Debye-Hückel activity model and thermodynamic database *PHREEQC.dat* (version 2.18.3) to calculate activity coefficients after adjusting Na^+ or Cl^- to achieve charge balance.

3. Monitoring Results

3.1. Groundwater Levels and Temperatures

All piezometer records show declining groundwater levels over the study period (Figure 2b). The mean rate of water table decline across all monitoring locations was 15 mm d^{-1} and was 17 mm d^{-1} at the location

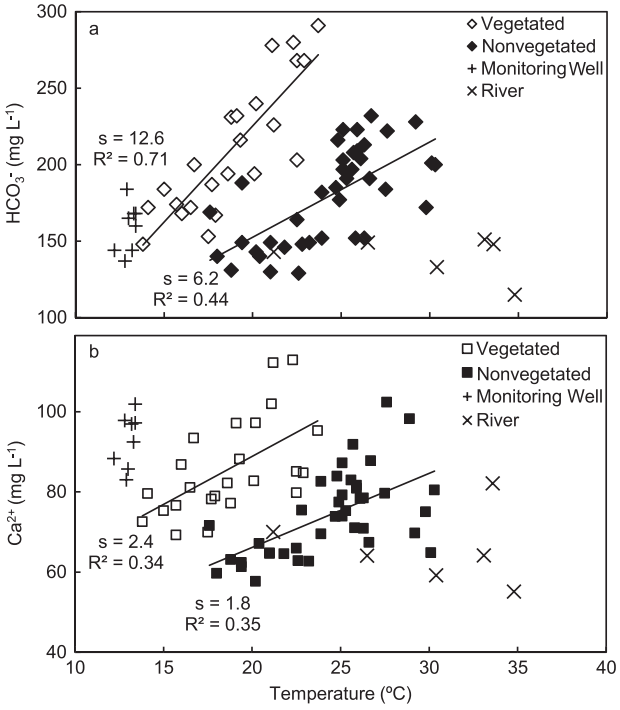

Figure 4. Both HCO_3^- and Ca^{2+} exhibit a correlation with temperature in each island. The highest slope ("s") and correlation is between HCO_3^- and temperature in the vegetated island. A one-way ANCOVA between the islands indicated that the slope of this correlation is significantly different. The difference in slope of the Ca^{2+} and temperature correlation is not significant between the islands.

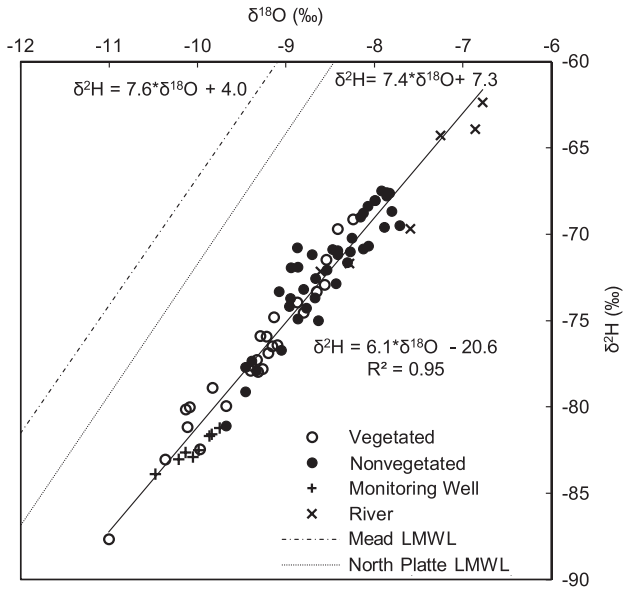

Figure 5. Stable isotopes of water for the islands, monitoring well, and river shown with the local meteoric water lines from Mead, NE, and North Platte, NE. The river water is the most isotopically enriched, while the monitoring well is generally the most depleted of all samples. Samples collected have a lower slope than the meteoric water, indicating evaporation after recharge.

that experienced the greatest decline (AN6). Vertical hydraulic gradients indicate downward groundwater flow throughout the study period, although the magnitude of downward flow and rate of water table decline varied spatially and temporally. In August 2012, a release from an upstream dam created a temporary increase in river discharge following several weeks of no flow in the river channel. Groundwater levels responded to this pulse between 6 August 2012 and 22 August 2012. Groundwater temperatures in both islands increased steadily through much of July 2012, after which they stabilized or decreased slightly (Figure 3a).

3.2. TDS, Major Ions, and Stable Isotopes

Total dissolved solids (TDS; estimated from electrical conductivity) generally ranged between 500 mg L^{-1} and 800 mg L^{-1} with an increasing trend over the study period (Figure 3b). All groundwater samples had Ca^{2+}-Na^+-HCO_3^--type hydrochemical facies. The mean percentage of HCO_3^- and SO_4^{2-} together was 84% of the total anion molarity. The mean percentage of cation molarity attributable to Ca^{2+} and Na^+ was 80%. HCO_3^-, Ca^{2+}, and Mg^{2+} represented most of the TDS increase (Figures 3d–3f). K^+ and Na^+ were less variable (see supporting information). HCO_3^- and Ca^{2+} had the strongest correlations with temperature among all measured ions (Figure 4). River water samples were generally more isotopically enriched than groundwater; samples from the 29 m deep monitoring well and the vegetated island were generally the least enriched (Figure 5). Linear regression indicates a $\delta^2H/\delta^{18}O$ slope of 6.1, which is lower than the local meteoric water line (LMWL) slope of 7.5 and implies an influence of evaporation on isotopic compositions (LMWL based on two stations within 220 km of the study area [*Harvey and Welker*, 2000; *Harvey*, 2001]). However, temporal variations in $\delta^{18}O$ and δ^2H did not indicate a consistent evaporation trend or directionally consistent mixing trend over the study period.

4. Discussion

4.1. Comparison Between Vegetated and Nonvegetated Islands

The mean rates of groundwater level decline were similar for vegetated and nonvegetated island monitoring locations; the decline rate was less than 1.5 mm d^{-1} higher in the nonvegetated island piezometers. Throughout the study period, piezometers on the vegetated island maintained cooler water temperatures (by as much as 10°C) than water temperatures in the nonvegetated island, and temperatures of deeper groundwater were cooler than shallower groundwater, as expected for summer months. It is likely that the higher vegetation density of the vegetated island inhibited insolation and led to overall slightly cooler water temperatures in the vegetated island. There was no notable difference in the water stable isotope values between the islands and groundwater, although the islands did generally appear isotopically distinct from the river. Neither island exhibited a temporal trend in conservative ion (Cl^-) concentration. The major ion with the strongest temporal trend was HCO_3^- in both islands. In addition, HCO_3^- and Ca^{2+} exhibited a positive correlation with temperature in both islands.

A one-way analysis of covariance (ANCOVA) was used to determine whether there were significant differences between the HCO_3^- or Ca^{2+} correlations with temperature between the islands. The ANCOVA indicated that the slopes of the temperature/HCO_3^- correlation between the vegetated and nonvegetated islands were significantly different ($p < 0.01$; Figure 4). Even when early season low temperatures in the nonvegetated island that are not representative of the broader temperature/HCO_3^- trend are removed from this calculation, the difference in the slopes is still significant at a level of $p = 0.05$. In contrast, there was no significant difference in the slope of the temperature/Ca^{2+} relationship between the islands ($p = 0.49$).

4.2. Carbonate System Impacts on Major Ion Trends

A major source of HCO_3^- in natural waters is the dissolution of CO_2 from the atmosphere or soil gas. Soil gas is a particularly important source considering that CO_2 in soil gas commonly reaches concentrations up to 100 times atmospheric partial pressure of carbon dioxide (pCO_2) [*Drake and Wigley*, 1975; *Reardon et al.*, 1979; *Kiefer and Amey*, 1992; *Hendry et al.*, 1999; *Jarvie et al.*, 2001; *Neal et al.*, 2002] through the combination of root (autotrophic) and microbial (heterotrophic) respiration (e.g., oxidation of organic matter). Heterotrophic and autotrophic respiration are referred to herein collectively as soil respiration. According to Henry's law, the dissolution of CO_2 and the formation of H_2CO_3 (carbonic acid) is proportional to pCO_2:

$$[H_2CO_3] = K_{CO2} * pCO_2 \quad (1)$$

where K_{CO2} is the temperature-dependent Henry's law coefficient for CO_2. The dissociation of H_2CO_3 is related to the thermodynamic constant K_{a1} and pH:

$$K_{a1} = \frac{[H^+][HCO_3^-]}{[H_2CO_3]} \quad (2)$$

Substituting equation (1) into equation (2) and solving for HCO_3^- illustrates that pCO_2 is related to HCO_3^- according to

$$[HCO_3^-] = \frac{[pCO_2] * K_{CO2} * K_{a1}}{[H^+]} \quad (3)$$

where K_{a1} is the temperature-dependent dissociation constant for H_2CO_3.

Simple equilibrium calculations suggest that as solution temperature increases, CO_2 solubility decreases, which subsequently leads to a decrease in HCO_3^- concentration (equation (1)). Therefore, if soil CO_2 was the source of HCO_3^- over the study period, an increase in gaseous pCO_2 sufficient to overcome the temperature effect on the Henry's law coefficient would be necessary to explain the observed increase in HCO_3^-. This is considered to be a plausible mechanism given that soil respiration rates have previously been found to be positively related to soil temperature [*Kiefer and Amey*, 1992; *Lloyd and Taylor*, 1994; *Hendry et al.*, 1999; *Karberg et al.*, 2005]. Although soil temperature was not measured in this study, the measured increase in water temperature (Figure 3a) is indicative of increasing soil temperatures. Other factors affecting soil

Table 1. Example PHREEQC Model Parameters

TITLE AN6-604	*Well AN6, 4 June 2012 Data*
units ppm	
temp 23	*Mean temperature*
O(0) 0	
pH 7.77	
Alkalinity 140 as HCO_3	
S(6) 226.1	
Cl 32.6	
Na 75.1 charge	*Charge balance parameter*
Ca 59.7	
K 11.4	
Mg 17.6	
EQUILIBRIUM_PHASES	
Calcite 0.38	*Mean saturation index*
REACTION	
CO_2 5e-3 moles in 200 steps	*Titration command*

respiration include soil moisture content [*Kiefer and Amey*, 1992; *Hendry et al.*, 1999], organic C availability [*Naganawa et al.*, 1989; *Kirschbaum*, 1995; *Bond-Lamberty and Thomson*, 2010], evapotranspiration, microbial populations, ambient CO_2 concentrations, and net primary productivity [*Brooke et al.*, 1983; *Lloyd and Taylor*, 1994; *Karberg et al.*, 2005].

PHREEQC [*Parkhurst and Appelo*, 1999] was used to calculate a soil zone pCO_2 value that, through equilibration with groundwater, would increase HCO_3^- by the amount measured in each piezometer. Modeling parameters included measured concentrations of all major ions and pH from each piezometer at the beginning of the study period, as well as the mean temperature from all sampling events at the piezometer and a fixed calcite saturation index, permitting calcite to be an equilibrium phase during the simulation (Table 1). Then, CO_2 was titrated into the simulated solution in 2.5×10^{-5} mol increments, simulating a gradual increase in pCO_2. At each step, new solution pH, ion, and CO_2 gas molarities were calculated. Also at each step, this output was used to calculate the equilibrium HCO_3^- concentration and theoretical soil gas pCO_2 using the solution CO_2 molarity and Henry's law. Each incremental CO_2 addition resulted in a new pH, ion, and CO_2 gas molarity output, as well as HCO_3^- and pCO_2 estimates. This process was repeated until the HCO_3^- molarity of the output solution was equivalent to the HCO_3^- concentration measured at the latest sampling event in each piezometer. A summary of the minimum and maximum temperatures and HCO_3^- measurements from the field are given with pCO_2 estimates from Henry's law in Table 2.

Solution chemistry for each piezometer was modeled at the mean temperature measured in that piezometer over the study. Henry's law coefficients for CO_2 were calculated for each piezometer after *Weiss* [1974] to account for different mean temperatures between piezometers. The model is moderately sensitive to temperature, and exclusive use of the mean temperature adds some uncertainty to the chemical output. The model is also sensitive to calcite saturation index, which was specified in the model according to the mean saturation index for all sampling events in a given piezometer over the study period. Solution pH was permitted to vary throughout the simulations.

The results of the geochemical modeling for each piezometer are shown in Figure 6. The open circles are the time series for HCO_3^- estimated from field alkalinity titrations. The dashed line represents the predicted HCO_3^- for shallow groundwater in equilibrium with increasing soil pCO_2 (shown on the upper *x* axis) and the water quality composition of samples from that piezometer at the beginning of the study. This model indicates that a relatively modest increase in soil pCO_2 could result in the measured change in groundwater HCO_3^-. The range of pCO_2 values needed for the given increase in HCO_3^- in each piezometer is reasonable for soil zone partial pressures [*Brooke et al.*, 1983; *Kiefer and Amey*, 1992]. Sufficient CO_2 production in the saturated zone appears less likely than CO_2 production in the unsaturated zone to cause the estimated increase in HCO_3^-, given that dissolved O_2 concentrations indicated suboxic

Table 2. Summary of Temperature, HCO_3^-, and pCO_2 Data[a]

	Vegetated			Nonvegetated					
	AV1	AV3	AV4	AN5	AN6	AN7	AN8	Monitoring Well	River
Temperature Min/Max (°C)	15.7/23.7	13.8/21.2	14.1/19.1	17.6/27.6	18.0/25.9	18.8/26.6	20.2/30.3	12.2/13.4	21.2/36.1
HCO_3^- Min/Max (mg/L)	153/291	148/278	172/232	146/232	129/223	130/223	143/228	137/184	115/168
Henry's law *p*CO2 Min/Max	2.5/2.0	2.5/1.8	2.3/2.0	2.6/2.2	2.9/2.4	2.6/2.0	2.7/2.1	-	-

[a]The pCO_2 was estimated in PHREEQC from pH and temperature measured in the field, and HCO_3^- is estimated from field titration.

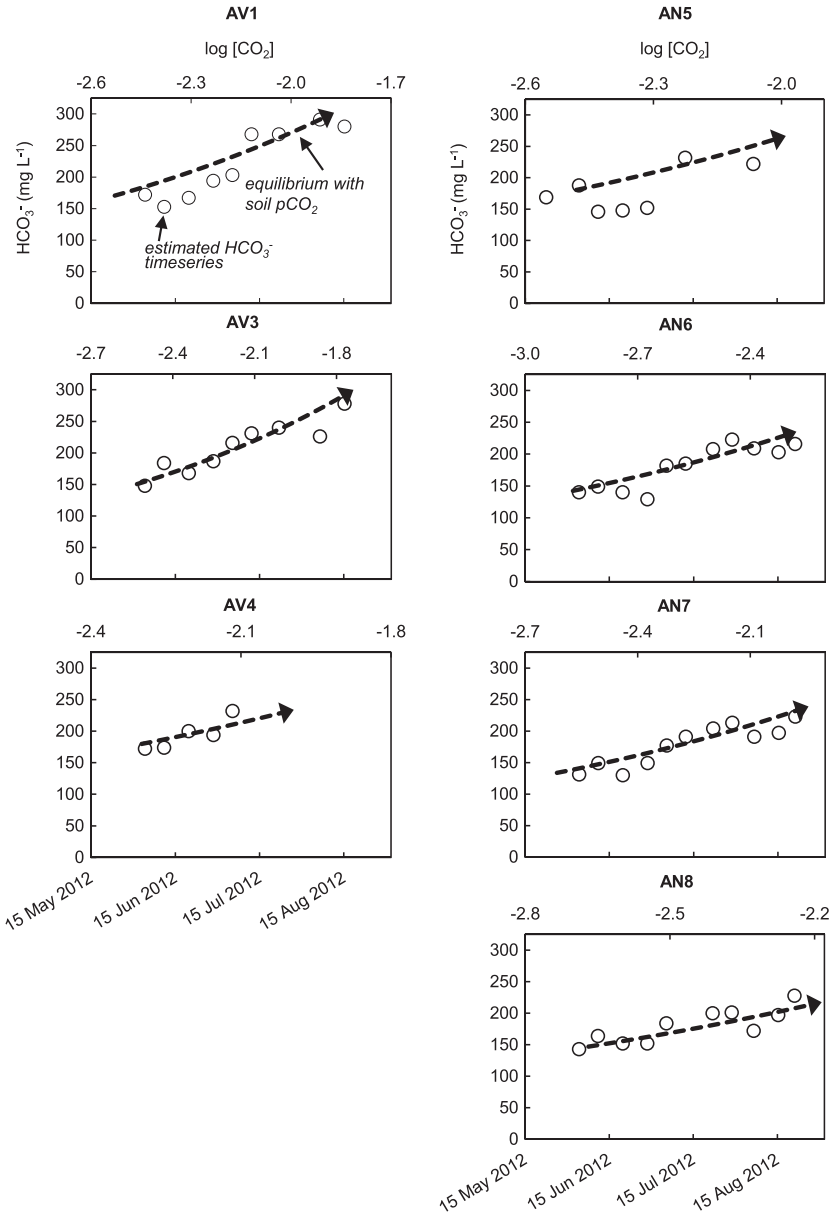

Figure 6. Thermodynamic equilibrium of shallow groundwater with soil pCO_2. Data points illustrate HCO_3^- measurements collected in each piezometer. The dashed line represents the equilibrium HCO_3^- concentration expected from a stepwise increase of CO_2 dissolution as a result of increased soil pCO_2 according to Henry's law.

conditions in the saturated zone and that concentrations of NO_3^- (another possible electron acceptor) were likely too low for significant organic matter oxidation to occur (mean island porewater concentration was $<1.3\ mg\ L^{-1}$ NO_3-N).

In order to determine the sensitivity of the proposed model to water temperature, HCO_3^- evolution was modeled at the approximate minimum and maximum temperatures at piezometer AN8, which underwent the greatest temperature increase of 10°C over the 3 month period (Figure 3a). The temperature sensitivity indicated in Figure 7 is largely attributable to the decreased solubility of calcite at higher temperatures. This calculation indicates that some of the difference in the measured HCO_3^- data from the modeled equilibrium line (Figure 6) may be attributable to the difference in the modeled temperature and the measured temperature at the time each sample was taken.

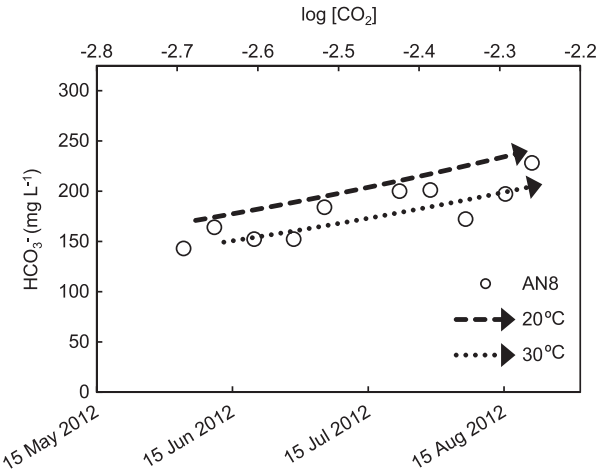

Figure 7. The equilibrium models are moderately sensitive to temperature. The difference in equilibrium CO_2 is shown here using the highest and lowest temperatures recorded in piezometer AN8 on the nonvegetated island. The difference can be attributed to lower solubility of calcite at higher water temperatures.

In addition to soil CO_2, another common source for HCO_3^- is the weathering of carbonate minerals such as calcite and dolomite [*Tsypin and Macpherson*, 2012]. For example,

$$\text{Calcite}: \quad H_2CO_3 + CaCO_3 \leftrightarrow Ca^{2+} + 2HCO_3^- \leftrightarrow Ca^{2+} + 2H^+ + 2CO_3^{2} \tag{R1}$$

$$\text{Dolomite}: \quad H_2CO_3 + CaMg(CO_3)_2 \leftrightarrow Ca^{2+} + Mg^{2+} + 2HCO_3^- \leftrightarrow Ca^{2+} + Mg^{2+} + 2H^+ + 2CO_3^{2-} \tag{R2}$$

Major ion concentrations can be used to infer whether CO_2 dissolution, carbonate weathering, or both processes contributed to the estimated HCO_3^- increase. In pure dissociation of carbonic acid, only the concentration of HCO_3^- is expected to increase, whereas the dissolution of calcite or dolomite (R1 and R2) should cause the sum of Ca^{2+} and Mg^{2+} to increase in a 1:1 molar ratio with HCO_3^-. In this study, Ca^{2+} and Mg^{2+} concentrations increased slightly in most piezometers over the study period (Figures 3e and 3f). Figure 8 shows the ratio of $Ca^{2+} + Mg^{2+}$: HCO_3^- to illustrate the relative changes in major carbonate ions. The slight overall decrease in the ratio of $Ca^{2+} + Mg^{2+}$: HCO_3^- over the study indicates that the increase in HCO_3^- only marginally outpaced the combined increase in Ca^{2+} and Mg^{2+}. This gives evidence for a contribution of carbonate mineral weathering to the overall HCO_3^- trend. A second possible source of Ca^{2+} would be cation exchange with Na^+ on clay mineral surfaces, which could account for the Na^+ decrease in piezometers AN6 and AN8 (see supporting information).

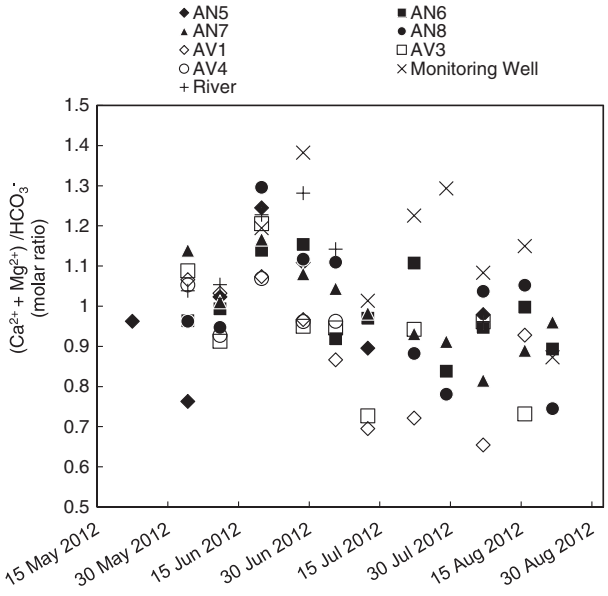

Figure 8. The molar ratio between carbonate system major cations and HCO_3^-. The slight decrease in the molar ratio suggests that Ca^{2+} and Mg^{2+} increased at a slightly higher rate than the increase in HCO_3^-, indicating that carbonate mineral weathering, rather than pure dissolution of H_2CO_3, likely contributed to the HCO_3^- increase over the study period.

Calculated saturation indices for calcite and dolomite suggest that both were slightly undersaturated in each of the piezometer

locations at the beginning of the study period. (Saturation index equals the log ratio of ion activity product and mineral solubility product; abbreviated SI). SI values for calcite and dolomite increased over the study period and were slightly supersaturated by the end of the study period (maximum calcite saturation indices ranged from 0.22 to 1.60 across monitoring locations; see supporting information). Whereas the increase in SI values is consistent with the mineral weathering hypothesis for increasing HCO_3^-, SI values greater than 0 are inconsistent with mineral-water equilibria. However, several other studies have found disequilibrium with respect to calcite in streams with relatively short residence times [*Suarez*, 1983; *Tobias and Böhlke*, 2011; *Lauerwald et al.*, 2013] and groundwater with longer residence times [*Amrhein and Suarez*, 1987; *Suarez et al.*, 1992; *Macpherson et al.*, 2008]. Disequilibrium in these studies has been attributed to slow calcite or dolomite precipitation kinetics relative to organic matter mineralization [*Reardon et al.*, 1979; *Amrhein and Suarez*, 1987], precipitation inhibition by dissolved organics or Mg^{2+} [*Suarez*, 1983], or a combination of both processes [*Suarez et al.*, 1992].

4.3. Alternative Hypotheses: Evaporative Concentration and Groundwater Mixing

One hypothesis for the observed increase in TDS and some major ions is that evaporation caused progressive concentration of the dissolved species. However, there was no definitive temporal trend in chloride concentration or stable isotopes (Figure 3c). These results are not consistent with evaporative concentration as a significant driver of increased ion concentrations in the shallow groundwater. First, chloride can be considered a conservative ion in this setting, and it is expected that increasing chloride concentrations would accompany any evaporative concentration of other ions; however, no clear temporal trend in Cl^- was found. It is possible that anthropogenic Cl^- sources (e.g., road salt) could be a confounding factor, but since this study was conducted in summer and the study location is surrounded by heavy agriculture, it is unlikely that any significant anthropogenic Cl^- sources to groundwater play a role in this case. Second, stable isotope evidence is not consistent with evaporative concentration as the main factor influencing increasing ion concentrations. Although river water, shallow groundwater, and deep groundwater samples all conform to a $\delta^2H/\delta^{18}O$ slope that is consistent with an evaporation signal relative to precipitation, temporal variability in isotopic values are not consistent with an enrichment trend over the study period. Rather, it is more likely that groundwater sampled during this study underwent evaporation prior to recharge. In particular, there is evidence that low $\delta^2H/\delta^{18}O$ slopes relative to local meteoric waters are common in the Platte River basin because of a combination of surface water evaporation from reservoirs and recycling of irrigation water. For example, *Böhlke et al.* [2007] found that the isotopic signature of the North Platte River and alluvial aquifer appeared evaporated relative to precipitation and attributed the lower regression slope of their respective samples to evaporation from upstream reservoirs. In summary, the available tracer evidence points to the streambed groundwater having undergone evaporative enrichment prior to recharge, but there is no evidence for subsequent evaporation from the streambed water table over the study period.

A second hypothesis for the TDS and HCO_3^- increase is mixing with groundwater that contains a higher concentration of HCO_3^- and Ca^{2+} and that proportionately more groundwater was present in the piezometers at the end of the season due to river flow decline. However, this hypothesis has several weaknesses, including the fact that only the carbonate system major ions demonstrated temporal trends, while other major ions (i.e., Cl^- and SO_4^{2-}) and stable isotopes did not. Additionally, groundwater HCO_3^- concentrations measured at the monitoring well are most similar to HCO_3^- measured in the piezometers in June 2012, early in the study, and do not closely represent the final carbonate system concentrations (Figure 4), the ratio of which should have contained more groundwater in a mixing scenario. Although it is possible that high-HCO_3^- and high-Ca^{2+} groundwater from a flow path that was not sampled at the monitoring well mixed with island porewater, the vertical hydraulic gradients at the piezometers indicated downward flow, suggesting that water from the hyporheic zone was moving away from the riverbed into the alluvial aquifer even during periods when water was flowing in the channel (see supporting information). While the data collected in this study therefore do not support a mixing scenario, additional investigation into the groundwater flow dynamics would be desirable to confirm this inference.

4.4. Mechanisms for Increasing pCO_2

The thermodynamic modeling results support the hypothesis that increased soil pCO_2 over the study period can explain the measured increase in groundwater HCO_3^-. However, there is uncertainty as to the

mechanism responsible for such an increase in soil pCO_2. As previously discussed, the two most likely sources of soil CO_2 are microbial and root respiration and both are stimulated by and therefore positively correlated to soil temperature. However, without separately measuring microbial or root respiration, their relative contributions to soil respiration as a whole is speculative [*Kirschbaum*, 2006]. It should also be noted that a potentially offsetting effect of increasing temperature on respiration is that soil dryness generally limits both primary productivity and microbial respiration; therefore, soil respiration in dry soil is less sensitive to temperature increases than in moist soils [*Howard and Howard*, 1993; *Reichstein et al.*, 2002; *Kirschbaum*, 2006]. In such cases, summer droughts may lead to less soil respiration than may be predicted by temperature alone [*Kirschbaum*, 1995]. Yet these small-scale results support the results of *Bond-Lamberty and Thomson* [2010], which indicated a positive correlation between the late twentieth century temperature anomaly and global soil respiration record, and demonstrate the potential impact of global climate change on groundwater DIC.

Two possible mechanisms are considered most likely for increasing respiration rates in the island unsaturated zone: (1) the seasonal increase in air temperature and (2) water table decline due to drought conditions exposing previously saturated sediments to oxygen. The first scenario, in the absence of moisture deficit, would be expected to increase both root and microbial respiration. The second scenario mainly impacts microbial respiration by creating aerobic conditions in previously saturated sediments. Comparison of trends for the vegetated island and nonvegetated island may provide some insight into whether any difference in the driver of increased pCO_2 exists between the islands. In particular, under these two scenarios, it would be expected that rates of HCO_3^- increase beneath vegetated islands would be greater than beneath nonvegetated islands because shallow streambed sediments beneath vegetated islands have substantially higher organic carbon content and root density. The results of the statistical analysis discussed above support this hypothesis, indicating that HCO_3^- did increase at a higher rate in the vegetated island. The slower, although still notable, increase in HCO_3^- with temperature in the nonvegetated island is likely attributable mostly to sediment drying and a subsequent increase in microbial respiration, as the root density on the island was significantly lower (only *de minimus* vegetation was present by the end of the study period).

Therefore, the overall temperature and chemical differences appear to be mainly attributable to the presence or absence of vegetative cover on each island. Given the insignificant root biomass and low soil organic content of the nonvegetated island, it may be that root respiration was an insignificant contributor to total soil respiration and that microbial respiration was the predominant CO_2 production mechanism in the nonvegetated island, although this process was not measured directly. In the vegetated island, it is likely that both root respiration and microbial respiration contributed to increased soil pCO_2, considering the high root density, organic-rich sediments, and water table decline.

5. Conclusion

The results of this study demonstrate the impacts of drought on shallow groundwater chemistry beneath a major braided stream in the midwestern U.S. (Platte River, Nebraska) following disconnection with the river. Thermodynamic equilibrium modeling suggests that increased temperatures associated with a 2012 drought event indirectly led to increasing trends in HCO_3^- and Ca^{2+} through enhanced root respiration or organic matter oxidation in the parafluvial zone. Based on available evidence from stable isotopes and major ions, the trends of increasing ion concentrations were not attributable to evaporation, groundwater mixing, or mineral-water reequilibria to increased temperature. Comparison of trends beneath vegetated and nonvegetated islands suggests that organic matter oxidation in the nonvegetated island progressed at a slower rate compared to root respiration and organic matter oxidation in the vegetated island, leading to a higher rate of HCO_3^- increase in the vegetated island. Future studies that can better control for the spatial distributions of parafluvial organic matter and vegetation cover are desirable in order to test this hypothesis.

This study highlights potential groundwater impacts near streams from the combination of seasonal transition and drought. Similar water quality responses to drought may be expected where shallow groundwater underlies temporarily dry riverbeds with significant organic carbon or vegetation cover. In view of predicted climate change, including higher frequency of heat waves in North America, it is

important to recognize that alluvial groundwater may (1) rapidly respond to environmental changes and (2) potentially serve as a carbon sink in cases where dissolved carbon concentrations increase as a result of those changes. Improved understanding of groundwater chemistry response to warm and dry conditions will help to better constrain terrestrial carbon budgets and impacts of environmental change.

Acknowledgments

Data supporting the results of this paper are available as supporting information. This material is based upon work supported by the National Science Foundation Graduate Research Fellowship under grant 25-0514-0142-001. This research was supported by additional funding from the Robert B. Daugherty Water for Food Institute, Geological Society of America, University of Nebraska (UNL) Department of Earth and Atmospheric Sciences, UNL Office of Graduate Studies, UNL Layman Fund, Nebraska Geological Society, American Association of Petroleum Geologists, and Phi Kappa Phi Honor Society. Field assistance was provided by Zablon Adane, Leilani Arthurs, Lindsey Bobak, Justin Gibson, Nathan Rossman, and J.P. Traylor. Field site access was granted by the Mary Lanning Hospital Trust and Crane Trust. The authors also thank Gwen Macpherson for her helpful review and comments.

References

Amrhein, C., and D. L. Suarez (1987), Calcite supersaturation in soils as a result of organic matter mineralization, *Soil Sci. Soc. Am. J.*, *51*(4), 932–937, doi:10.2136/sssaj1987.03615995005100040020x.

Andrews, J. A., and W. H. Schlesinger (2001), Soil CO_2 dynamics, acidification, and chemical weathering in a temperate forest with experimental CO_2 enrichment, *Global Biochem. Cycles*, *15*(1), 149–162, doi:10.1029/2000GB001278.

Appelo, C. A. J., M. J. J. Van Der Weide, C. Tournassat, and L. Charlet (2002), Surface complexation of ferrous iron and carbonate on ferrihydrite and the mobilization of arsenic, *Environ. Sci. Technol.*, *36*, 3096–3103, doi:10.1021/es010130n.

Böhlke, J. K., I. M. Verstraeten, and T. F. Kraemer (2007), Effects of surface-water irrigation on sources, fluxes, and residence times of water, nitrate, and uranium in an alluvial aquifer, *Appl. Geochem.*, *22*, 152–174, doi:10.1016/j.apgeochem.2006.08.019.

Bond-Lamberty, B., and A. Thomson (2010), Temperature-associated increases in the global soil respiration record, *Nature*, *464*(7288), 579–582, doi:10.1038/nature08930.

Borken, W., Y. J. Xu, R. Brumme, and N. Lamersdorf (1999), A climate change scenario for carbon dioxide and dissolved organic carbon fluxes from a temperate forest soil: Drought and rewetting effects, *Soil Sci. Soc. Am. J.*, *63*(6), 1848–1855, doi:10.2136/sssaj1999.6361848x.

Boulton, A. J., S. Findlay, P. Marmonier, E. H. Stanley, and H. M. Valett (1998), The functional significance of the hyporheic zone in streams and rivers, *Annu. Rev. Ecol. Syst.*, *29*(59), 59–81.

Brooke, G. A., M. E. Folkoff, and E. O. Box (1983), A world model of soil carbon, *Earth Surf. Processes Landforms*, *8*(1), 79–88, doi:10.1002/esp.3290080108.

Brunke, M., and T. Gonser (1997), The ecological significance of exchange processes between rivers and groundwater, *Freshwater Biol.*, *37*(1), 1–33.

Chen, X. (2007), Hydrologic connections of a stream-aquifer-vegetation zone in south-central Platte River valley, Nebraska, *J. Hydrol.*, *333*(2), 554–568, doi:10.1016/j.jhydrol.2006.09.020.

Chen, X. (2011), Depth-dependent hydraulic conductivity distribution patterns of a streambed, *Hydrol. Processes*, *25*, 278–287.

Chen, X., and L. Shu (2006), Groundwater evapotranspiration captured by seasonally pumped wells in river valleys, *J. Hydrol.*, *318*(1–4), 334–347.

Chen, X., W. Dong, G. Ou, Z. Wang, and C. Liu (2013), Gaining and losing stream reaches have opposite hydraulic conductivity distribution patterns, *Hydrol. Earth Syst. Sci.*, *17*(7), 2569–2579, doi:10.5194/hess-17-2569-2013.

Cheng, C., J. Song, X. Chen, and D. Wang (2011), Statistical distribution of streambed vertical hydraulic conductivity along the Platte River, Nebraska, *Papers in Natural Resources*, Paper 362.

Ciais, P., et al. (2005), Europe-wide reduction in primary productivity caused by the heat and drought in 2003, *Nature*, *437*, 529–533.

Cole, J. J., et al. (2007), Plumbing the global carbon cycle: Integrating inland waters into the terrestrial carbon budget, *Ecosystems*, *10*, 171–184.

Cornic, G., and C. Fresneau (2002), Photosynthetic carbon reduction and carbon oxidation cycles are the main electron sinks for photosystem II activity during a mild drought, *Ann. Bot.*, *89*, 887–894.

Drake, J. J., and T. M. L. Wigley (1975), The effect of climate on the chemistry of carbonate groundwater, *Water Resour. Res.*, *11*, 958–962, doi:10.1029/WR011i006p00958.

Eaton, B. C., R. G. Millar, and S. Davidson (2010), Channel patterns: Braided, anabranching, and single-thread, *Geomorphology*, *120*, 353–364.

Eschner, T. R., R. F. Hadley, and K. D. Crowley (1983), Hydrologic and morphologic changes in channels of the Platte River basin in Colorado, Wyoming, and Nebraska: A historical perspective, in *Hydrologic and Geomorphic Studies of the Platte River Basin*, *U.S. Geol. Surv. Prof. Pap.*, vol. 1277, edited by T. R. Eschner et al., chap. A1-A39, U.S. Geol. Surv., Washington, D. C.

Harvey, F. E. (2001), Use of NADP archive samples to determine the isotope composition of precipitation: Characterizing the meteoric input function for use in groundwater studies, *Ground Water*, *39*(3), 380–390.

Harvey, F. E., and J. M. Welker (2000), Stable isotopic composition of precipitation in the semi-arid north-central portion of the U.S. Great Plains, *J. Hydrol.*, *238*(1–2), 90–109, doi:10.1016/S0022-1694(00)00316-4.

Hendry, M. J., C. A. Mendoza, R. A. Kirkland, and J. R. Lawrence (1999), Quantification of transient CO_2 production in a sandy unsaturated zone, *Water Resour. Res.*, *35*(7), 2189–2198, doi:10.1029/1999WR900060.

Horn, J. D., R. M. Joeckel, and C. R. Fielding (2012), Progressive abandonment and planform changes of the central Platte River in Nebraska, central USA, over historical timeframes, *Geomorphology*, *139*, 372–383.

Howard, D. M., and P. J. A. Howard (1993), Relationships between CO_2 evolution, moisture-content and temperature for a range of soil types, *Soil Biol. Biochem.*, *25*(11), 1537–1546.

Hurr, T. E. (1983), Groundwater hydrology of the Mormon Island Crane Meadows wildlife area near Grand Island, Hall County, Nebraska, in *Hydrologic and Geomorphic Studies of the Platte River Basin*, *U.S. Geol. Surv. Prof. Pap.*, vol. 1277, pp. H1–H12, U.S. Geol. Surv., Washington, D. C.

Jahangir, M. M. R., P. Johnston, M. I. Khalil, D. Hennessy, J. Humphreys, O. Fenton, and K. G. Richards (2012), Groundwater: A pathway for terrestrial C and N losses and indirect greenhouse gas emissions, *Agric. Ecosyst. Environ.*, *159*, 40–48.

Jarvie, H. P., C. Neal, R. Smart, R. Owen, D. Fraser, I. Forbes, and A. Wade (2001), Use of continuous water quality records for hydrograph separation and to assess short-term variability and extremes in acidity and dissolved carbon dioxide for the River Dee, Scotland, *Sci. Total Environ.*, *265*, 85–98.

Karberg, N. J., K. S. Pregitzer, J. S. King, A. L. Friend, and J. R. Wood (2005), Soil carbon dioxide partial pressure and dissolved inorganic carbonate chemistry under elevated carbon dioxide and ozone, *Oecologia*, *142*(2), 296–306.

Kessler, T. J., and C. F. Harvey (2001), The global flux of carbon dioxide into groundwater, *Geophys. Res. Lett.*, *28*, 279–282, doi:10.1029/2000GL011505.

Kiefer, R. H., and R. G. Amey (1992), Concentrations and controls of soil carbon dioxide in sandy soil in the North Carolina Coastal Plain, *Catena*, *19*(6), 539–559, doi:10.1016/0341-8162(92)90052-D.

Kilpatrick, J. M. (1996), Temporal changes in the configuration of the water table in the vicinity of the management systems evaluation area site, central Nebraska, *Water-Resour. Invest. Rep. 94-4173*, U.S. Geol. Surv., Washington, D. C.

Kirschbaum, M. U. F. (1995), The temperature dependence of soil organic matter decomposition, and the effect of global warming on soil organic C storage, *Soil Biol. Biochem.*, *27*(6), 753–760.
Kirschbaum, M. U. F. (2006), The temperature dependence of organic-matter decomposition—Still a topic of debate, *Soil Biol. Biochem.*, *38*(9), 2510–2518.
Lane, S. (1995), The dynamics of dynamic river channels, *Geography*, *80*(2), 147–162.
Lauerwald, R., J. Hartmann, N. Moosdorf, S. Kempe, and P. A. Raymond (2013), What controls the spatial patterns of the riverine carbonate system?—A case study for North America, *Chem. Geol.*, *337–338*, 114–127.
Leopold, L. B., and M. G. Wolman (1957), *River Channel Patterns: Braided, Meandering and Straight*, *U.S. Geol. Surv. Prof. Pap.*, vol. 282-B, U.S. Geol. Surv., Washington, D. C.
Liu, Z., and J. Zhao (1999), Contribution of carbonate rock weathering to the atmospheric CO_2 sink, *Environ. Geol.*, *39*, 1053–1058.
Liu, Z., W. Dreybrodt, and H. Wang (2010), A new direction in effective accounting for the atmospheric CO_2 budget: Considering the combined action of carbonate dissolution, the global water cycle and photosynthetic uptake of DIC by aquatic organisms, *Earth Sci. Rev.*, *99*, 162–172.
Lloyd, J., and J. A. Taylor (1994), On the temperature-dependence of soil respiration, *Funct. Ecol.*, *8*(3), 315–323, doi:10.2307/2389824.
Macpherson, G. L. (2009), CO_2 distribution in groundwater and the impact of groundwater extraction on the global C cycle, *Chem. Geol.*, *264*, 328–336, doi:10.1016/j.chemgeo.2009.03.018.
Macpherson, G. L., J. A. Roberts, J. M. Blair, M. A. Townsend, D. A. Fowle, and K. R. Beisner (2008), Increasing shallow groundwater CO_2 and limestone weathering, Konza Prairie, USA, *Geochim. Cosmochim. Acta*, *72*, 5581–5599.
Medlyn, B. E. (2011), Comment on "Drought-induced reduction in global terrestrial net primary production from 2000-2009", *Science*, *333*, 1093-d.
Meehl, G. A., and C. Tebaldi (2004), More intense, more frequent, and longer lasting heat waves in the 21st Century, *Science*, *305*, 994–997.
Naganawa, T., K. Kyuma, H. Yamaoto, Y. Yamamoto, H. Yokoi, and K. Tatsuyama (1989), Measurement of soil respiration in the field: Influence of temperature, moisture level, and application of sewage sludge compost and agro-chemicals, *Soil Sci. Plant Nutr.*, *35*(4), 509–516.
National Climatic Data Center (NCDC) (2013), National Climatic Data Center Global Historical Climatology Network-Grand Island Weather Station, Ashville, N. C. [Available at http://www.ncdc.noaa.gov/.]
National Climatic Data Center (NCDC) (2014), National temperature and precipitation maps, June-August 2012, Ashville, N. C. [Available at http://www.ncdc.noaa.gov/temp-and-precip/maps.php.]
Neal, C., C. Watts, R. J. Williams, M. Neal, L. Hill, and H. Wickham (2002), Diurnal and longer term patterns in carbon dioxide and calcite saturation for the River Kennet, south-eastern England, *Sci. Total Environ.*, *282–283*, 205–231.
Parkhurst, D. L., and C. A. J. Appelo (1999), *User's Guide to PHREEQC (Version 2)—A Computer Program for Speciation, Batch-reaction, One-dimensional Transport, and Inverse Geochemical Calculations*, *Water-Resour. Invest. Rep.*, vol. 99–4259, U.S. Geol. Surv., Denver, Colo.
Peckenpaugh, J. M., and J. T. Dugan (1983), *Hydrogeology of Parts of the Central Platte and Lower Loup Natural Resources Districts, Nebraska*, *Water-Resour. Invest. Rep.*, vol. 83–4219, 125 pp., U.S. Geol. Surv., Lincoln, Nebraska.
Piégay, H., G. Grant, F. Nakamura, and N. Trustrum (2006), Braided river management: From assessment of river behavior to improved sustainable development, in *Braided Rivers: Process, Deposits, Ecology, and Management*, *IAS Spec. Publ.*, vol. 36, edited by G. H. Sambrook-Smith et al., pp. 257–275, Intl. Assoc. of Sediment., Oxford, U. K.
Raymond, P. A., and J. J. Cole (2003), Increase in the export of alkalinity from North America's Largest River, *Science*, *301*(5629), 88–91.
Reardon, E. J., G. B. Allison, and P. Fritz (1979), Seasonal chemical and isotopic variations of soil CO_2 at Trout Creek, Ontario, *J. Hydrol.*, *43*, 335–371.
Reichstein, M., J. D. Tenhunen, O. Roupsard, J. Ourcival, S. Rambal, F. Miglietta, A. Peressottis, M. Pecchiaris, G. Tiron, and R. Valentini (2002), Severe drought effects on ecosystem CO_2 and H_2O fluxes at three Mediterranean evergreen sites: Revision of current hypotheses?, *Global Change Biol.*, *8*, 999–1017.
Richey, J. E., A. V. Krusche, M. S. Johnson, H. B. da Cunha, and M. V. Ballester (2009), The role of rivers in the regional carbon balance, *Amazonia Global Change Geophys. Monogr. Ser.*, *186*, 489–504.
Suarez, D. L. (1983), Calcite supersaturation and precipitation kinetics in the Lower Colorado River, All-American Canal and East Highline Canal, *Water Resour. Res.*, *19*, 653–661, doi:10.1029/WR019i003p00653.
Suarez, D. L., J. D. Wood, and I. Ibrahim (1992), Reevaluation of calcite supersaturation in soils, *Soil Sci. Soc. Am. J.*, *56*, 1776–1784.
Tobias, C., and J. K. Böhlke (2011), Biological and geochemical controls on diel dissolved inorganic carbon cycling in a low-order agricultural stream: Implications for reach scales and beyond, *Chem. Geol.*, *283*, 18–30.
Tsypin, M., and G. L. Macpherson (2012), The effect of precipitation events on inorganic carbon in soil and shallow groundwater, Konza Prairie LTER Site, NE Kansas, USA, *Appl. Geochem.*, *27*, 2356–2369.
Weiss, R. F. (1974), Carbon dioxide in water and seawater: The solubility of a non-ideal gas, *Mar. Chem.*, *2*, 203–215.
Williams, A. J., C. B. Andersen, and G. P. Lewis (2009), Evaluating the effects of sample processing treatments on alkalinity measurements, *J. Hydrol.*, *377*, 455–464, doi:10.1016/j.jhydrol.2009.09.007.
Williams, G. P. (1978), *The Case of the Shrinking Channels—The North Platte and Platte Rivers in Nebraska*, *Geol. Surv. Circ.*, vol. 781, Washington, D. C.
Worrall, F., and A. Lancaster (2005), The release of CO_2 from riverwaters—The contribution of excess CO_2 from groundwater, *Biogeochemistry*, *76*, 299–317.
Xie, X., Y. Wang, and C. Su (2012), Hydrochemical and sediment biomarker evidence of the impact of organic matter biodegradation on arsenic mobilization in shallow aquifers of Datong Basin, China, *Water Air Soil Pollut.*, *223*(2), 483–498.
Yan, J., Y. P. Wang, G. Zhou, S. Li, G. Yu, and K. Li (2011), Carbon uptake by karsts in the Houzhai Basin, southwest China, *J. Geophys. Res.*, *116*, G04012, doi:10.1029/2011JG001686.
Zeng, N., and H. Qian (2005), Impact of 1998–2002 midlatitude drought and warming on terrestrial ecosystem and the global carbon cycle, *Geophys. Res. Lett.*, *32*, L22709, doi:10.1029/2005GL024607.
Zhao, M., and S. W. Running (2010), Drought-induced reduction in global terrestrial net primary production from 2000 through 2009, *Science*, *329*(5994), 940–943.